

# Rapid Melting and Solidification of a Surface Due to a Moving Heat Flux

S. KOU, S. C. HSU, AND R. MEHRABIAN

Rapid melting and solidification of a semi-infinite substrate subjected to a high intensity heat flux over a circular region on its bounding surface moving with a constant velocity is considered. General expressions are developed for the coefficients in the finite difference equation governing the heat transfer in moving orthogonal curvilinear coordinate systems. These expressions are reduced to their specific forms in terms of dimensionless nodal temperature and enthalpy for a moving oblate spheroidal coordinate system. Quasisteady state conditions are assumed and the thermal properties of the substrate in the liquid and solid phase are considered constant and equal. It is also assumed that the substrate melts and solidifies at a single temperature. Temperature distributions in the molten region and the adjacent heat affected zone are computed along with the liquid-solid interface shape, its velocity and other important solidification variables. Both uniform and Gaussian heat flux distributions within the circular region are considered. The results are presented in their most general form—in terms of dimensionless numbers when possible. Specific criteria for the melting of the substrate are established. It is shown that the three variables, absorbed heat flux  $q$ , the radius of the circular region  $a$  and the velocity of the moving flux  $U$ , could be combined into two independent variables. That is, the dimensionless temperature distribution in the metal pool and the solid substrate remain the same as long as the products  $qa$  and  $Ua$  or  $U/q$  are kept constant. The effect of these variables on cooling rate in the liquid and the ratio of temperature gradient to growth rate at the solid-liquid interface are discussed using an aluminum substrate as an example.

## I. INTRODUCTION

THE availability of high power directed energy sources such as the electron beam and different types of lasers has led to the development of a number of new materials processing techniques which exploit the unique characteristics of these sources. One such process, the rapid surface layer melting and subsequent solidification of metallic and semiconductor substrates, appears to have many potential applications. In two recent papers<sup>1,2</sup> we addressed the one and two dimensional transient heat flow problems during rapid melting and solidification of the surface of a semi-infinite substrate subjected to a high intensity stationary heat flux on its bounding surface. In the present investigation the earlier findings are extended to three-dimensional heat flow on the surface of a semi-infinite solid subjected to a moving heat flux. It is anticipated that the equations and solution method developed would be equally applicable to other metallurgical processes such as welding.

In general, most experiments with a directed energy source, such as the continuous wave CO<sub>2</sub> laser, involve

scanning of the source over the surface of the substrate. Analytical solutions to simple moving heat source problems have previously been considered by Rosenthal.<sup>3</sup> His analysis is for a solid substrate which does not undergo a phase change. It is based on the notion that if the dimensions of the substrate are large with respect to the moving source, then the system approaches a quasisteady state; steady state prevails from the standpoint of an observer located in and travelling with the source. The analytical solutions of Rosenthal<sup>3</sup> have been extensively used in metallurgical processes such as welding and surface hardening. However, these solutions are only accurate at large distances from the source and can not address the complex problem of melting and solidification which is the subject of this investigation.

In this paper we extend the mathematical technique developed and used in the previous two-dimensional transient heat flow problem.<sup>2</sup> The oblate spheroidal coordinate system is used again, however, the mathematical expressions and computer methodology developed assume the existence of a quasisteady state while the coordinate system is in motion (*i.e.* after the starting transients have vanished).

## II. PROBLEM STATEMENT AND SOLUTION APPROACH

We consider a high intensity heat flux over a circular region on the bounding surface of a semi-infinite solid moving with a constant velocity,  $U$ , in the  $y$ -direction in cartesian coordinate system, Fig. 1. The absorbed heat flux is high enough to cause melting of the surface layer.

S. KOU and S. C. HSU, formerly Research Associate and Graduate Student, respectively, at the University of Illinois, Urbana, Illinois are now Assistant Professor, Department of Metallurgy and Materials Science, Carnegie-Mellon University, Pittsburgh, Pennsylvania, and Technical Staff Member at G. T. E. Laboratories, Waltham, Massachusetts. R. MEHRABIAN, formerly Professor in the Department of Metallurgy and Mining Engineering and the Department of Mechanical and Industrial Engineering, University of Illinois, Urbana, Illinois is now Chief of the Metallurgy Division at the National Bureau of Standards, Department of Commerce, Washington, D.C.

Manuscript submitted March 20, 1979.

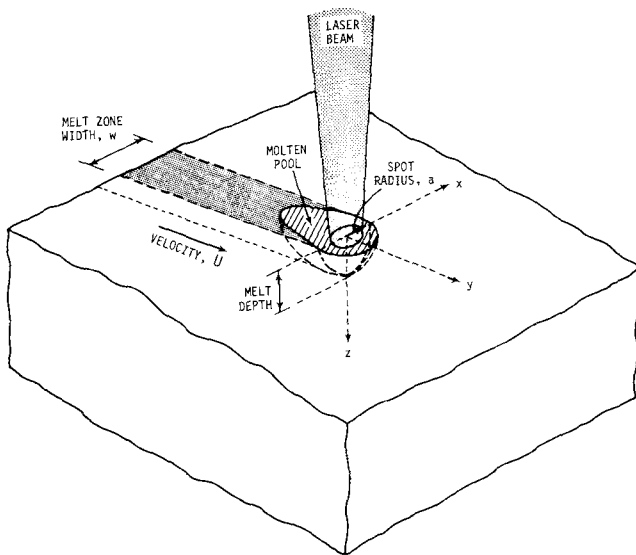


Fig. 1—Schematic illustration of a laser beam—substrate geometry during rapid surface melting and solidification.

Temperature profiles in the molten region and the adjacent heat affected zone, as well as the important melting and solidification variables of the surface layer are to be determined. The analysis is based on the assumption that a quasisteady state is established, which is to say that the system appears to be in a steady state as viewed by an observer located at the center of the circular region and travelling with the heat source. We thus transfer the coordinate system from the semi-infinite solid to the center of the heat source. The surface outside the heated region is considered adiabatic. The thermal properties of the solid and the liquid phases are considered to be constant and equal. Finally, it is assumed that the workpiece melts and solidifies at a single temperature.

The generalized expressions previously derived<sup>4</sup> for the determination of the coefficients in the finite difference equations governing the stationary heat transfer problem within discretized spatial domains are extended to account for the motion of orthogonal curvilinear coordinate systems. These expressions are then reduced to their specific forms for a moving oblate spheroidal coordinate system which is a “more natural” coordinate system than the cartesian for this problem geometry. The finite difference equations are rewritten in terms of dimensionless nodal enthalpy and temperature, in a manner similar to that previously described,<sup>2,6</sup> to permit numerical solution of the multi-dimensional, discrete temperature-phase change problem. In this way, both dimensionless temperature and enthalpy are used to formulate a single energy conservation equation for each discretized spatial domain regardless of whether it is in the solid state, the liquid state or contains the liquid-solid interface. Finally, the quasisteady state temperature distributions in the molten region and the adjacent heat affected zone are computed along with the liquid-solid interface shape, its velocity and other important melting and solidification variables; cooling rate and the ratio of temperature gradient in the liquid to the interface velocity.

### III. MATHEMATICAL DESCRIPTION

The generalized form of the heat conduction equation in stationary orthogonal curvilinear coordinate system  $(u_1, u_2, u_3)$  has previously been derived. For a volume element moving in space with velocities  $v_1, v_2$  and  $v_3$  this expression can be expanded to include conduction of heat in and out of the volume element due to motion:\*

\*All the terms in the equations are defined in the Nomenclature.

$$\begin{aligned} & \frac{\partial}{\partial u_1} \left[ \frac{k_1 h}{h_1^2} \frac{\partial T}{\partial u_1} \right] + \frac{\partial}{\partial u_2} \left[ \frac{k_2 h}{h_2^2} \frac{\partial T}{\partial u_2} \right] \\ & + \frac{\partial}{\partial u_3} \left[ \frac{k_3 h}{h_3^2} \frac{\partial T}{\partial u_3} \right] + P \cdot h = \rho \frac{\partial}{\partial t} (hH) \\ & - \rho \left[ \frac{h}{h_1} v_1 \frac{\partial H}{\partial u_1} + \frac{h}{h_2} v_2 \frac{\partial H}{\partial u_2} + \frac{h}{h_3} v_3 \cdot \frac{\partial H}{\partial u_3} \right] \end{aligned} \quad [1]$$

Where the scalar factors (metric coefficients) relating the curvilinear coordinate system to the cartesian system are those previously defined.<sup>5</sup> The arc lengths, areas and the volume of the element in the curvilinear coordinates are related to the cartesian by:

$$ds_i = h_i du_i; \quad i = 1, 2, 3 \quad [2]$$

$$dA_i = h_j h_k du_j du_k; \quad i, j, k = 1, 2, 3 \quad [3]$$

$$dV = h du_1 du_2 du_3 \quad [4]$$

Finally,  $P$  in Eq. [1] denotes source strength per unit volume.

The Taylor series expansion of Eq. [1] about an arbitrary discretized domain in space centered at a node at  $(i, j, k)$  can now be carried out to put the equation in

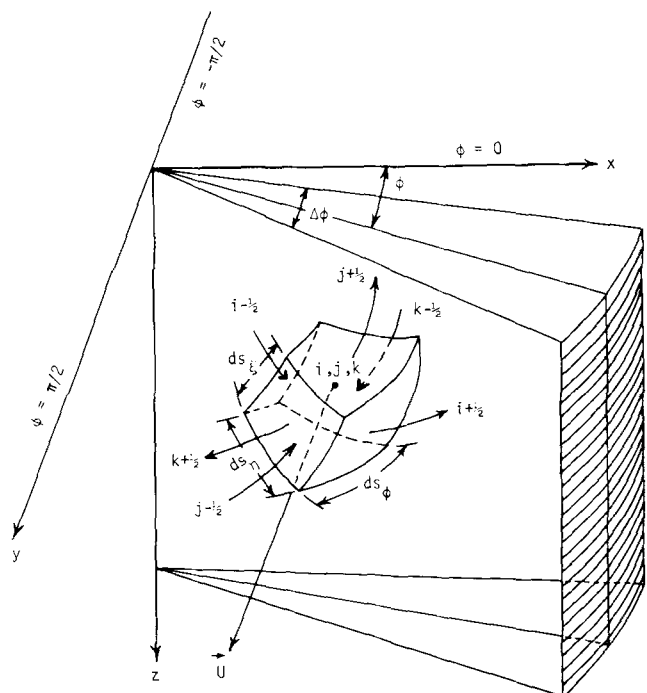


Fig. 2—Three-dimensional moving oblate spheroidal coordinate system and problem geometry showing a discretized space domain.

finite difference form. The subscripts  $i, j$  and  $k$  indicate the finite discretization of space in the  $u_1, u_2$  and  $u_3$  directions, respectively. The change in respective coordinate values between successive nodes are  $\Delta u_1, \Delta u_2$

and  $\Delta u_3$ . If terms of the order of  $\Delta u^3$  and higher are neglected, the substitution of all the finite difference approximations in Eq. [1] yields the coefficients to the various nodal temperatures:

$$\begin{aligned}
 & \left[ \frac{k_1 h}{h_1^2 \Delta u_1^2} - \frac{1}{2 \Delta u_1} \frac{\partial}{\partial u_1} \left( \frac{k_1 h}{h_1^2} \right) \right] T_{i-1, j, k} - \frac{1}{2 \Delta u_1} \left( \frac{\rho h v_1}{h_1} \right) \Big|_{i, j, k} H_{i-1, j, k} \\
 & + \left[ \frac{k_2 h}{h_2^2 \Delta u_2^2} - \frac{1}{2 \Delta u_2} \frac{\partial}{\partial u_2} \left( \frac{k_2 h}{h_2^2} \right) \right] T_{i, j-1, k} - \frac{1}{2 \Delta u_2} \left( \frac{\rho h v_2}{h_2} \right) \Big|_{i, j, k} H_{i, j-1, k} \\
 & + \left[ \frac{k_3 h}{h_3^2 \Delta u_3^2} - \frac{1}{2 \Delta u_3} \frac{\partial}{\partial u_3} \left( \frac{k_3 h}{h_3^2} \right) \right] T_{i, j, k-1} - \frac{1}{2 \Delta u_3} \left( \frac{\rho h v_3}{h_3} \right) \Big|_{i, j, k} H_{i, j, k-1} \\
 & + \left[ \frac{k_1 h}{h_1^2 \Delta u_1^2} + \frac{1}{2 \Delta u_1} \frac{\partial}{\partial u_1} \left( \frac{k_1 h}{h_1^2} \right) \right] T_{i+1, j, k} + \frac{1}{2 \Delta u_1} \left( \frac{\rho h v_1}{h_1} \right) \Big|_{i, j, k} H_{i+1, j, k} \\
 & + \left[ \frac{k_2 h}{h_2^2 \Delta u_2^2} + \frac{1}{2 \Delta u_2} \frac{\partial}{\partial u_2} \left( \frac{k_2 h}{h_2^2} \right) \right] T_{i, j+1, k} + \frac{1}{2 \Delta u_2} \left( \frac{\rho h v_2}{h_2} \right) \Big|_{i, j, k} H_{i, j+1, k} \\
 & + \left[ \frac{k_3 h}{h_3^2 \Delta u_3^2} + \frac{1}{2 \Delta u_3} \frac{\partial}{\partial u_3} \left( \frac{k_3 h}{h_3^2} \right) \right] T_{i, j, k+1} + \frac{1}{2 \Delta u_3} \left( \frac{\rho h v_3}{h_3} \right) \Big|_{i, j, k} H_{i, j, k+1} \\
 & + \left[ -2 \left( \frac{k_1 h}{h_1^2 \Delta u_1^2} + \frac{k_2 h}{h_2^2 \Delta u_2^2} + \frac{k_3 h}{h_3^2 \Delta u_3^2} \right) \Big|_{i, j, k} \right] T_{i, j, k} - \left( \frac{h \rho}{\Delta t} \right) \Big|_{i, j, k} H_{i, j, k} \\
 & + \left[ P \cdot h + \left( \frac{h \rho H^0}{\Delta t} \right) \right] \Big|_{i, j, k} = 0
 \end{aligned} \tag{5}$$

Application of the general Expression [5] to a moving oblate spheroidal coordinate system located at the center of the heat flux and travelling with the source is now considered. The cartesian and the oblate spheroidal coordinate systems are shown in Fig. 2. The heat flux is applied over a circular region of radius  $a$  in the  $x$ - $y$  plane and is travelling in the  $y$ -direction with constant velocity  $U$ .

$$\begin{aligned}
 v_y &= U \\
 v_x &= v_z = 0
 \end{aligned} \tag{6}$$

The thermal properties are considered to be uniform isotropic and equal for the solid and liquid phase. Quasisteady state conditions are assumed—terms involving time in Eq. [5] are zero.

The control volume is centered about an arbitrary point  $(i, j, k)$  in space and is moving with a velocity  $U$  in the positive  $y$ -direction.  $i, j$  and  $k$  indicate the finite discretization of space in the  $\eta, \xi$  and  $\phi$  directions, respectively.

$$\begin{aligned}
 u_1 &= \eta, u_2 = \xi, u_3 = \phi \\
 v_1 &= v_\eta, v_2 = v_\xi, v_3 = v_\phi
 \end{aligned} \tag{7}$$

The scalar factors (metric coefficients) for the oblate spheroidal coordinates and the interrelationship between vector components (velocities) in the two coordinate systems are given in Ref. [5]. Substituting Eq. [6] in these interrelationships and performing the indicated

operations yields:

$$\begin{aligned}
 v_\eta &= \frac{U \sinh \eta \sin \xi \sin \phi}{\sqrt{\cosh^2 \eta - \sin^2 \xi}} \\
 v_\xi &= \frac{U \cosh \eta \cos \xi \sin \phi}{\sqrt{\cosh^2 \eta - \sin^2 \xi}} \\
 v_\phi &= U \cos \phi
 \end{aligned} \tag{8}$$

The scalar factors and the velocity components from Ref. [5] are now used in the general expressions for the finite difference coefficients.<sup>5</sup> Once the appropriate operations are carried out Expression [5] can be put in a more useful form for the problem at hand.

$$\begin{aligned}
 C_s T_{i, j, k} &= C_1 T_{i-1, j, k} + C_2 T_{i+1, j, k} + C_3 T_{i, j-1, k} \\
 &+ C_4 T_{i, j+1, k} + C_5 T_{i, j, k-1} + C_6 T_{i, j, k+1} \\
 &- \frac{C_7}{C_p} H_{i-1, j, k} + \frac{C_8}{C_p} H_{i+1, j, k} - \frac{C_9}{C_p} H_{i, j-1, k} \\
 &+ \frac{C_{10}}{C_p} H_{i, j+1, k} - \frac{C_{11}}{C_p} H_{i, j, k-1} + \frac{C_{12}}{C_p} H_{i, j, k+1} \\
 &+ \frac{Pa(\cosh^2 \eta_i - \sin^2 \xi_j)}{k}
 \end{aligned} \tag{9}$$

The coefficients in Eq. [9] are:

$$\begin{aligned}
 C_{1,2} &= \frac{1}{\Delta \eta^2} \mp \frac{1}{2 \Delta \eta} \tanh \eta_i \\
 C_{3,4} &= \frac{1}{\Delta \xi^2} \mp \frac{1}{2 \Delta \xi} \cot \xi_j
 \end{aligned}$$

$$\begin{aligned}
C_{5,6} &= \frac{1}{\Delta\phi^2} \frac{(\cosh^2\eta_i - \sin^2\xi_j)}{\cosh\eta_i \sin^2\xi_j} \\
C_7 = C_8 &= \frac{aU\rho C_p}{2k\Delta\eta} \sinh\eta_i \sin\xi_j \sin\phi_k \\
C_9 = C_{10} &= \frac{aU\rho C_p}{2k\Delta\xi} \cosh\eta_i \cos\xi_j \sin\phi_k \\
C_{11} = C_{12} &= \frac{aU\rho C_p}{2k\Delta\phi} \frac{(\cosh^2\eta_i - \sin^2\xi_j)}{\cosh\eta_i \sin\xi_j} \cos\phi_k \\
C_s = \sum_{n=1}^6 C_n &= +2 \left[ \frac{1}{\Delta\eta^2} + \frac{1}{\Delta\xi^2} + \frac{1}{\Delta\phi^2} \frac{(\cosh^2\eta_i - \sin^2\xi_j)}{\cosh^2\eta_i \sin^2\xi_j} \right]
\end{aligned} \tag{10}$$

In the above each coefficient has been divided by ( $ak \cosh\eta_i \sin\xi_j \Delta\eta\Delta\xi\Delta\phi$ ).

The finite difference representation of the heat conduction equation can now be put in its equivalent enthalpy form using a modified version of notation in Ref. [2] for dimensionless nodal enthalpy,  $\psi$ , and dimensionless nodal temperature,  $\theta$ . These two dependent variables are defined as:

$$\begin{aligned}
\psi &= \frac{1}{\rho V} \int_V \rho \frac{(H - H_s^*)}{\Delta H_{sl}} dV = \frac{H - H_s^*}{\Delta H_{sl}} \\
\theta &= C_p \frac{(T - T_M)}{\Delta H_{sl}}
\end{aligned} \tag{11}$$

In general,  $H$  in Eq. [11] refers to the specific enthalpy of the discretized space volume and assumes different forms when the node is in the liquid, the solid or the liquid-solid region.  $H_s^*$  is the specific enthalpy of the solid at its melting point.

In the solid region the dimensionless nodal enthalpy,  $\psi$ , is negative and is equal to the dimensionless nodal temperature:

$$\psi = \theta = \frac{C_p(T - T_M)}{\Delta H_{sl}} < 0 \tag{12}$$

In the superheated liquid region:

$$\begin{aligned}
\psi &= 1 + \frac{C_p(T - T_M)}{\Delta H_{sl}} > 1.0 \\
\theta &= \psi - 1
\end{aligned} \tag{13}$$

A discretized space volume containing the liquid-solid interface is at the melting point of the material:

$$0 \leq \psi \leq 1.0 \quad \text{and} \quad \theta = 0 \tag{14}$$

The value of  $\psi$  is equal to the weight fraction of the element which is in the liquid state,  $f_l$ .

The appropriate forms of Eq. [11] for a discretized space domain in the solid or liquid region, Eqs. [12] or [13] are substituted into Eq. [9]. After some manipulation and multiplication by different factors the following common equation is obtained for both the solid and the liquid.

$$\begin{aligned}
C_s \psi_{i,j,k} &= C_1 \theta_{i-1,j,k} + C_2 \theta_{i+1,j,k} + C_3 \theta_{i,j-1,k} \\
&+ C_4 \theta_{i,j+1,k} + C_5 \theta_{i,j,k-1} + C_6 \theta_{i,j,k+1} \\
&- C_7 \psi_{i-1,j,k} + C_8 \psi_{i+1,j,k} - C_9 \psi_{i,j-1,k} \\
&+ C_{10} \psi_{i,j+1,k} - C_{11} \psi_{i,j,k-1} + C_{12} \psi_{i,j,k+1} \\
&+ C_s f_{L,i,j,k} + \frac{Pa^2(\cosh^2\eta_i - \sin^2\xi_j)}{k} \cdot \frac{C_p}{\Delta H_{sl}}.
\end{aligned} \tag{15}$$

The coefficients  $C_1$  to  $C_{12}$  and  $C_s$  are those defined in Expression [10].

An alternate approach to the general formulation of the problem developed here, which results in Eqs. [9] and [10], is to apply an energy balance to an arbitrary moving control volume of finite size with a total source strength  $P\Delta V$  centered about node  $i, j, k$  in oblate spheroidal coordinates. This approach, described in detail in the Appendix, is very useful because; a) it verifies the general formulation of Eq. [1] developed in this investigation, and b) it renders improved physical interpretations of the various coefficients derived for Eq. [9] and [10] and the boundary conditions described in the next section.

#### IV. BOUNDARY CONDITIONS AND SOLUTION OF THE FINITE DIFFERENCE EQUATIONS

The boundary conditions are derived based on the following assumptions.

The absorbed heat flux in the circular region of the bounding surface ( $z = 0$ ,  $x$ - $y$  plane) is in general a function of distance and time,  $q = q(r, t)$  where  $r = \sqrt{x^2 + y^2}$ . In this paper the problem is solved for the two special cases of uniform and Gaussian distributions of the absorbed heat flux within the circular region. Equation [15] is then subject to the following boundary conditions.

$$\begin{aligned}
\text{I. } \eta &= 0, \quad 0 \leq \xi \leq \pi/2, \\
-\frac{\pi}{2} &\leq \phi \leq \frac{\pi}{2}, \quad \frac{\partial T}{\partial \eta} = 0
\end{aligned} \tag{16}$$

The first node at this boundary is at  $i = 1$ ,  $\eta_1 = \Delta\eta/2$ , therefore, the surface located at  $i - 1/2$  is coincident with this boundary of symmetry:

$$Q_{i-1/2,j,k}|_{i=1} = 0, \quad C_1 = 0 \tag{17}$$

Similarly, the top surface is parallel to the moving direction, hence:

$$C_7 = 0 \tag{18}$$

In general, the heat flux in the circular region on the bounding surface is incorporated in the term involving  $P$  in Eq. [15].

$$P = \frac{\text{rate of heat generated}}{\text{unit volume}} = \frac{a^2}{2} \frac{\int_{\xi_j - \Delta\xi/2}^{\xi_j + \Delta\xi/2} q(\xi) \sin(2\xi) d\xi \cdot \int_{\phi - \Delta\phi/2}^{\phi + \Delta\phi/2} d\phi}{\Delta V} \tag{19}$$

where  $\Delta V$  is the volume of the discretized space domain.

$$\Delta V = h\Delta\eta\Delta\xi\Delta\phi = a^3(\cosh^2\eta_i - \sin^2\xi_j) \times \cosh\eta_i \sin\xi_j \Delta\eta\Delta\xi\Delta\phi \quad [20]$$

For case a)  $q = \text{constant}$

$P$  is calculated from Eqs. [19] and [20]. Substitution of this finding in the last term of Eq. [15] leads to the following expression:

$$\frac{aq \cos\xi_j \sin(\Delta\xi)}{k \cosh\eta_i \Delta\eta\Delta\xi} \times \frac{C_p}{\Delta H_{st}} \quad [21]$$

$$\text{For case b) } q = q_0 e^{-2\sin^2\xi_j} \quad [22]$$

and the last term of Eq. [15] becomes:

$$\frac{q_0 a [e^{-2\sin^2(\xi_j - \frac{\Delta\xi}{2})} - e^{-2\sin^2(\xi_j + \frac{\Delta\xi}{2})}]}{4 k \cos h\eta_i \sin \xi_j \Delta\eta\Delta\xi} : \frac{C_p}{\Delta H_{st}} \quad [23]$$

$$\text{II. } \eta > 0, \quad 0 \leq \xi \leq \pi/2,$$

$$\phi = -\pi/2, \quad \frac{\partial T}{\partial \phi} = 0, \quad P = 0 \quad [24]$$

(the negative  $y$  portion of the  $y$ - $z$  plane,  $x = 0$ )

Because of problem symmetry about the  $y$ - $z$  plane the plane defined by  $\phi = -\pi/2$  will represent a zero flux boundary. Since the first node at this boundary is at  $k = 1$ ,  $\phi_1 = \Delta\phi/2$ , then the surface located at  $k - 1/2$  is coincident with this boundary of symmetry:

$$Q_{i,j,k-1/2}|_{k=1} = 0, \quad C_5 = 0 \quad [25]$$

Similarly, this surface is parallel to the moving direction; hence:

$$C_{11} = 0 \quad [26]$$

$$\text{III. } \eta > 0, \quad 0 \leq \xi \leq \frac{\pi}{2},$$

$$\phi = +\frac{\pi}{2}, \quad \frac{\partial T}{\partial \phi} = 0, \quad P = 0 \quad [27]$$

(the positive  $y$  portion of the  $y$ - $z$  plane,  $x = 0$ )

By using a similar reasoning to that given above we must set

$$C_6 = 0, \quad C_{12} = 0 \quad [28]$$

$$\text{IV. } \eta \rightarrow \infty, \quad 0 < \xi < \pi/2,$$

$$-\pi/2 < \phi < \pi/2, \quad P = 0 \quad [29]$$

Far away from the circular region (for the problem at hand,  $\eta \rightarrow 10$ ):

$$\theta_{i,j,k} = \psi_{i,j,k} = \frac{-C_p(T_M - T_o)}{\Delta H_{st}} \quad [30]$$

$$\text{V. } \eta > 0, \quad \xi = 0, \quad P = 0 \quad [31]$$

(along the  $z$ -axis,  $x = 0, y = 0$ )

The area of the surface located at  $j - 1/2$  along this

boundary is zero:

$$C_3 = 0, \quad C_9 = 0 \quad [32]$$

$$\text{VI. } \eta > 0, \quad \xi = \pi/2,$$

$$-\pi/2 < \phi < \pi/2, \quad P = 0 \quad [33]$$

The surface on the  $x$ - $y$  plane outside the circular region is adiabatic:

$$Q_{i,j+1/2,k}|_{j=\text{Max}} = 0, \quad C_4 = 0 \quad [34]$$

The top surface is parallel to the moving direction, hence:

$$C_{10} = 0 \quad [35]$$

The system of quasisteady state algebraic equations, Eq. [15], in the moving oblate spheroidal coordinates were solved using an iterative method. The computer logic presented below closely follows that previously described for the two-dimensional transient heat flow problem for stationary heat flux applied in the circular region on the surface of a semi-infinite solid.<sup>2</sup> However, the quasisteady state nature of the problem has eliminated time derivatives from the heat flow equation.

The solution is started by initially assigning a temperature of  $T_o$  to the semi-infinite solid. Then, by using Eqs. [12] to [14] the left hand side, LHS of Eq. [15] is calculated using the boundary conditions by repeated point iteration throughout the mesh in a definite order a number of times until the convergence criterion is met. The following logic is used in the sequence of calculations.

If  $\psi_{i,j,k} < 0$  the element is in the solid and right hand side, RHS, of Eq. [15] is less than zero.

$$\psi_{i,j,k} = \frac{\text{RHS}}{C_s} \quad [36]$$

As the calculation is repeated for the next nodal point, the value of  $\theta$  in the previous nodal point in the mesh is set equal to that calculated from Eq. [36]. On the other hand, if  $0 \leq \psi_{i,j,k} \leq 1.0$  the element contains the liquid-solid interface and the value calculated from Eq. [36] gives the fraction of liquid in the volume element. The value of  $\theta$  for this nodal point is set equal to zero in the next iteration step. Finally, if  $\psi_{i,j,k} > 0$  the element is in the superheated liquid region and the values of  $\phi$  and of  $\theta$  for this nodal point become that given by Eq. [13].

The convergence criteria is tested by comparing the new value of  $\psi_{i,j,k}$  with the old guess value:

$$|\psi_{i,j,k}(\text{new}) - \psi_{i,j,k}(\text{old})| \leq 10^{-4} \quad [37]$$

Convergence is assumed when Eq. [37] is satisfied.

## V. RESULTS AND DISCUSSION

The equations and the computer logic developed were used to calculate the quasisteady state temperature distribution in an aluminum\* substrate subjected to

\* The properties of aluminum used in the calculations are listed in Table I.

both uniform and Gaussian moving heat flux distri-

butions. The results are presented in their most general form, when possible, *i.e.* in terms of dimensionless parameters in order to establish general trends between the process variables and the important melting and solidification parameters. The sequence of the presentation is as follows. First, the steady state temperature distributions due to a stationary heat flux acting over a circular region of radius  $a$  are discussed and the results are compared with the transient heat flow calculations of the previous paper.<sup>2</sup> It is shown that the criteria developed earlier, between the product of the absorbed heat flux and the radius of the circular region  $qa$  and the steady state temperature at the center of the circular region, are equally applicable to the problem on hand. A significant departure from the earlier<sup>2</sup> calculations is the assumption that the conductivities of the liquid and the solid phases are equal. The effect of this assumption on the steady state temperature distributions is discussed. Secondly, the effect on the temperature distributions and the solidification parameters of moving the heat flux in the  $y$ -direction with a dimensionless velocity  $Ua/2\alpha$  are discussed in detail for both uniform and Gaussian heat flux distributions.

### 1. Steady State Temperature Distributions Stationary Heat Flux

Figure 3 shows a general plot of the data obtained in the previous study.<sup>2</sup> The curve associated with the vertical axis on the right side of this figure shows that there is a minimum product of  $qa$  required if the center of the circular region on the surface of the substrate is to reach a given temperature, *e.g.* the vaporization temperature of the substrate. That is, for very small values of  $a/2\sqrt{\alpha t}$  (long interaction times) the temperature at this location approaches its maximum steady state value. Again, the term  $\Delta H_{sl}/C_p$  in the numerator on the right hand vertical axis of Fig. 3 denotes the equivalent temperature change for the melting of the substrate.

For the aluminum substrate, the minimum values of  $qa \approx 1.45 \times 10^5$  W/m and  $qa \approx 2.3 \times 10^5$  W/m are deduced from Fig. 3 for a solid surface temperature  $T(0,0,0) = T_M$  and for the initiation of surface melting, respectively. These values are identical to those of the previous calculations.<sup>2</sup> On the other hand, the minimum

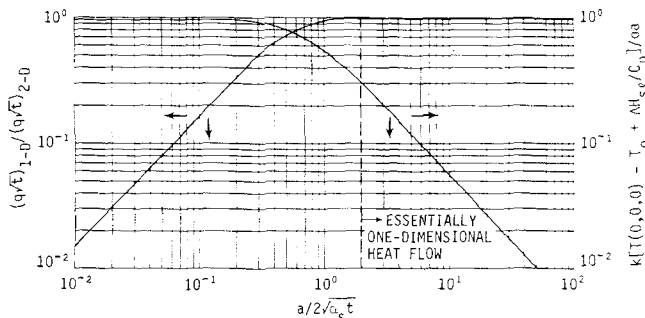


Fig. 3—Temperature at the center of the liquid zone of a semi-infinite solid substrate during surface melting as a function of uniform absorbed heat flux, radius of the circular region and time from Ref. [2].

value of  $qa \approx 6.4 \times 10^5$  W/m deduced for the center of the circular region to reach the vaporization temperature is larger than that calculated earlier because the assumed higher conductivity of the liquid\* permits

\* The higher conductivity of the solid is used for both the liquid and the solid in this study. The actual average conductivity of the liquid is  $108 \text{ W m}^{-1} \text{ K}^{-1}$ .

rather diffusion of heat away from the heat source.

Figure 4 shows the effect of different thermal conductivity values on the location of the liquid-solid interface when steady state prevails. Note that a higher liquid conductivity, while the conductivity of the solid remains the same, results in a larger metal pool (a higher  $qa$  value) if the center of the circular region is to reach the vaporization temperature.

The steady state temperature distributions of a stationary heat source are of interest because this is the problem geometry as the velocity of the moving heat source approaches zero. Figure 5 shows the shape and location of several isotherms, including the liquid-solid interface, in an aluminum substrate for two different values of the product  $qa$ . These are steady state isotherms and the center of the circular region has reached maximum temperatures  $T_v$  and 2130 K for  $qa = 6.4 \times 10^5$  W/m and  $qa = 5 \times 10^5$  W/m, respectively. The temperature distributions remain the same in these dimensionless plots for all values of  $q$  and  $a$  as long as the product  $qa$  is kept constant.

Figure 6 shows the effect of increasing the product  $qa$  on the steady state location of the liquid-solid interface. The associated maximum temperature at the center of the circular region is listed on each curve. The melt pool becomes deeper and hotter as the product of the uniform absorbed heat flux and the radius of the circular region increases. Furthermore, ratio of the melt width to the melt depth is larger than one and increases with decreasing value of the product  $qa$ .

Figures 7 and 8 show the actual temperature distri-

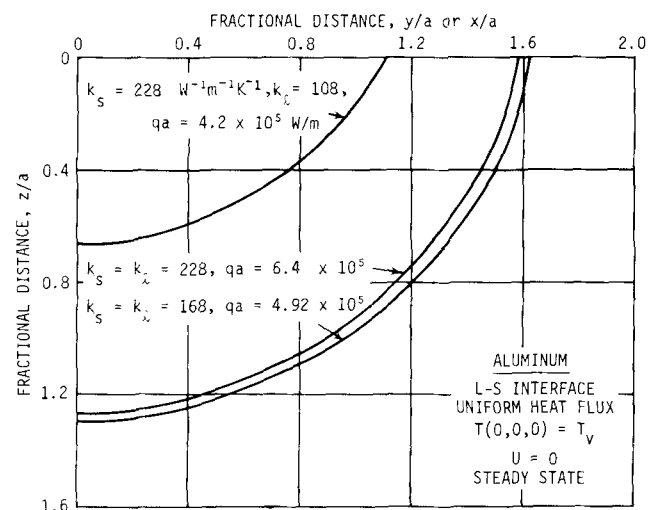


Fig. 4—The effect of changes in the thermal conductivities of the liquid and solid phases on the steady state location of the liquid-solid interface of an aluminum substrate subjected to a stationary uniform absorbed heat flux  $q$  over a circular region of radius  $a$ . In each case the center of the circular region has reached the vaporization temperature  $T_v$ .

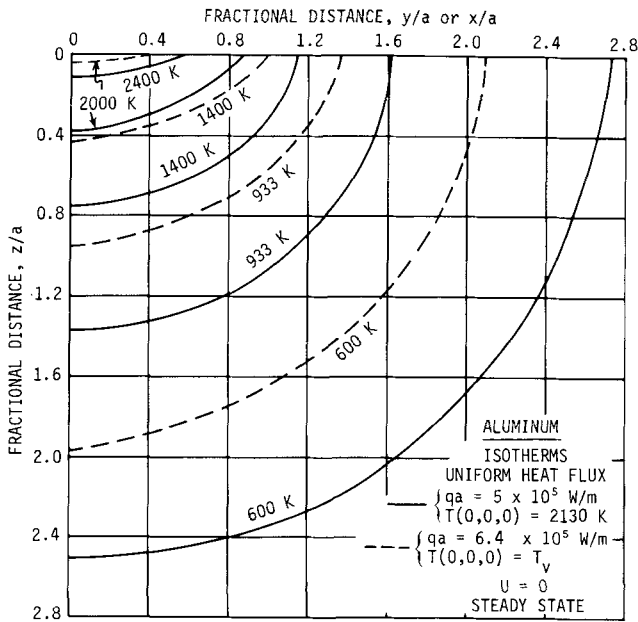


Fig. 5—Steady state location of several isotherms, including the liquid-solid interface ( $T = 993$  K) for two different products of  $qa$ .

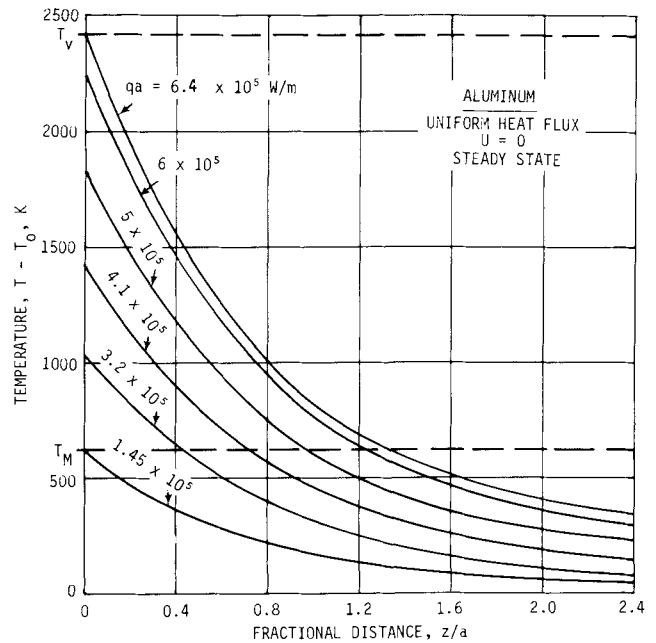


Fig. 7—Steady state temperature distributions in the melt pool and the solid along the  $z$ -axis for different values of the variable  $qa$ .

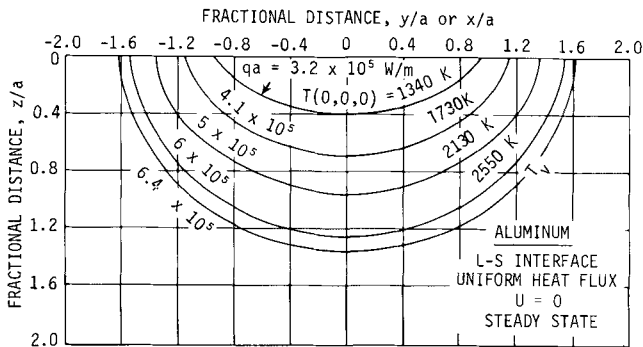


Fig. 6—The effect of the variable  $qa$  on the steady state geometry and location of the liquid-solid interface. The maximum temperature at the center of the circular region associated with each curve is also listed.

butions in the melt pool and the solid along the  $z$ -axis and on the  $z = 0$  plane, respectively. As anticipated, temperature gradients along the  $z$ -axis increase with increasing values of the product  $qa$  and decrease with increasing distance from the surface of substrate. On the other hand, symmetry on the  $z = 0$  plane requires a zero temperature gradient with respect to the  $x$  or the  $y$  axis at the center of the circular region. Note that the temperature gradients at the edge of the pool on this plane increase with decreasing values of the product  $qa$ . This information will be of interest when relationships between cooling rates and process variables are discussed in the moving heat flux problem geometry.

## 2. Quasisteady State Heat Flow— Moving Heat Flux

**A. Uniform Heat Flux.** An initial finding of this investigation was that the three variables, absorbed heat flux  $q$ , the radius of the circular region  $a$  and the velocity of the moving heat flux  $U$ , could be combined into two independent variables. That is, the dimension-

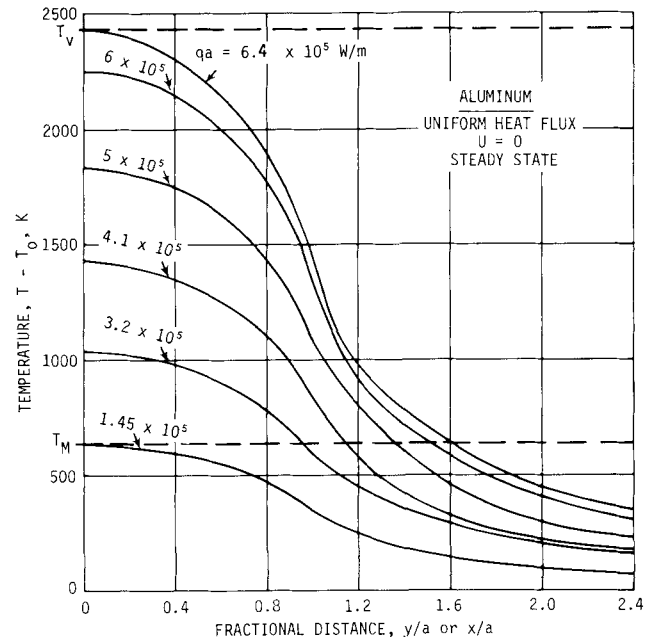


Fig. 8—Steady state radial temperature distributions in the melt pool on the  $z = 0$  plane for different values of the variable  $qa$ .

Table I. Properties of the Aluminum Substrate

$C_p^*$	= 1067	J Kg <sup>-1</sup> K <sup>-1</sup> , specific heat
$\Delta H_{sl}$	= $3.95 \times 10^5$	J Kg <sup>-1</sup> , latent heat of fusion
$K_{\dagger}$	= 228	Wm <sup>-1</sup> K <sup>-1</sup> , thermal conductivity
$T_M$	= 933	K, melting temperature
$T_v$	= 2723	K, vaporization temperature
$\rho^*$	= 2545	Kg m <sup>-3</sup> density
$\alpha$	= $8.4 \times 10^{-5}$	m <sup>2</sup> s <sup>-1</sup> , thermal diffusivity

\* Averaged from 298 K to the vaporization temperature.

† Averaged from 298 K to melting temperature.

less temperature distribution in the liquid metal pool and the solid substrate remain the same as long as the products  $qa$  and  $Ua$  or  $U/q$  are kept constant while the individual values of the three variables are varied. Consequently, the data is presented herein in a general form, covering a large range of process parameters, in terms of the product  $qa$  or  $U/q$  and the dimensionless parameter  $Ua/2\alpha$ . The latter parameter has previously been used in crystal growth models.<sup>7,8</sup>

Figure 9 shows the dimensionless temperature distribution along the  $y$ -axis for different values of  $Ua/2\alpha$ . For small values of  $Ua/2\alpha \sim 0.003$  the heat flux is moving very slowly across the substrate in the  $y$ -direction and the temperature distributions are almost, but not exactly, identical to those shown in Figs. 5 to 8. That is, there is little distortion of the melt pool and it remains almost symmetrical as it travels across the substrate. On the other hand, increasing the dimensionless velocity results in increasing distortion of the metal pool—the maximum temperature along the  $y$ -axis shifts toward the tail end of the pool. The data in Fig. 9 permits determination of temperature distribution along the  $y$ -axis for a wide range of process variables. For example, for a radius of the circular region  $a = 400 \mu\text{m}$  and  $qa = 6.4 \times 10^5 \text{ W/m}$  the maximum temperature reached at steady state,  $U = 0$ , was the vaporization temperature of aluminum. The maximum dimensionless velocity  $Ua/2\alpha \sim 1.0$  in Fig. 9 translates into an actual velocity of  $\sim 0.42 \text{ m/s}$ , a temperature  $T(0,0,0) \sim 2400 \text{ K}$  and a maximum temperature, displaced from the center of the circular region,  $T_{\text{max}} \approx 2540 \text{ K}$ . Changing the product  $qa$  to  $4.1 \times 10^5 \text{ W/m}$  while  $Ua/2\alpha$  is kept constant, results in a significant reduction in the temperature at the origin  $T(0,0,0) \sim 1510 \text{ K}$ —compare this with the steady state value of  $1730 \text{ K}$  in Fig. 6.

Examples of the shape and location of several isotherms, including the liquid-solid interface, for given values of the products  $qa$  and  $Ua/2\alpha$  are shown in Fig. 10. This figure shows composite top and side views of the isotherms at steady state for a stationary and a moving heat source.

The dimensionless velocity  $Ua/2\alpha = 0.75$  would, for example, translate into actual velocities of  $0.1 \text{ m/s}$  and  $1 \text{ m/s}$  for radii of the circular region of  $\sim 1260 \mu\text{m}$  and  $\sim 126 \mu\text{m}$ , respectively. The corresponding absorbed uniform heat fluxes that result in  $qa = 6.4 \times 10^5 \text{ W/m}$  are  $q \sim 5.1 \times 10^8 \text{ W/m}^2$  and  $q \sim 5.1 \times 10^9 \text{ W/m}^2$ , respectively. Figure 10 shows significant shifts in the geometry of the isotherms to the trailing end of the moving heat source.

It is interesting to note that due to the high conductivity of the aluminum substrate the distortions in the isotherms are not nearly as pronounced as those expected in lower conductivity materials such as iron or nickel. This point was clearly demonstrated in the moving point source calculations of Rosenthal.<sup>3</sup>

Figures 11 and 12 show the effects of changing the variables  $qa$  and  $Ua/2\alpha$  on the geometry and location of the liquid-solid interface—the liquid pool. First, it is evident that there is little distortion of the pool at low velocities. Second, increasing the product  $Ua/2\alpha$  results in a corresponding decrease in a maximum pool depth.

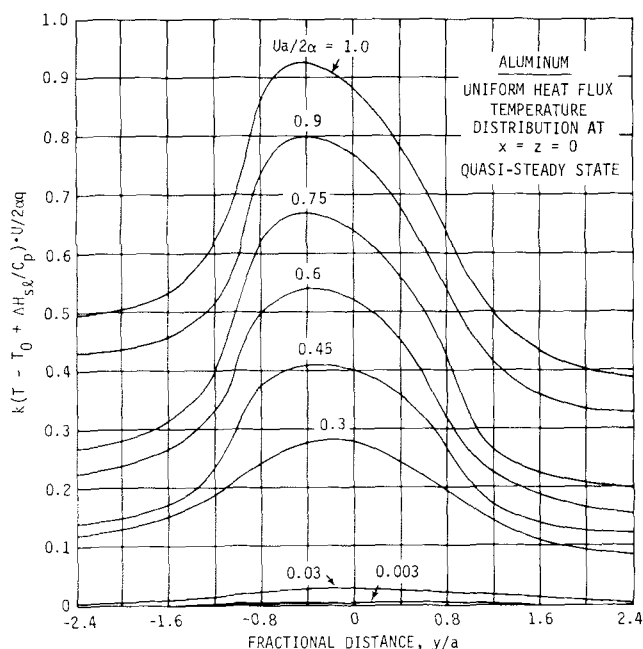


Fig. 9—Quasisteady state dimensionless temperature distributions along the  $y$ -axis of a moving uniform heat flux  $q$  absorbed over a circular region of radius  $a$ . The velocity of the heat source,  $U$ , is in the positive  $y$ -direction.

Third, the geometry of the pool is more spherical at higher products of  $qa$ —its width to depth ratio increases with decreasing values of  $qa$ . Finally, shallower pool geometries are less affected by changes in the dimensionless velocity.

The effect of changes in the values of  $qa$  and  $Ua/2\alpha$  on the cooling rate in the liquid at the solid-liquid interface,  $G_L \cdot R$ ,\* and the variation of this cooling

\*  $G_L$  and  $R$  are the temperature gradient in the liquid and the solid-liquid interface velocity perpendicular to the metal pool surface, respectively.

rate along the different axes of the cartesian coordinates are shown in Figs. 13 and 14. These are calculated cooling rates during solidification of the trailing half of the metal pool. Heating and cooling rates from the point of view of a stationary observer located anywhere in the heat affected zone of the substrate can similarly be determined. The cooling rate,  $G_L \cdot R$ , can be alternatively described as the producer of  $U \cdot \partial T / \partial y$ , where  $\partial T / \partial y$  is the  $y$ -component of the temperature gradient in the liquid at the liquid-solid interface. The cooling rate is a maximum along the  $y$ -axis and its value for a given radius of the circular region increases with increasing values of the ratio  $U/q$ . This is clearly evident in the plots of Figs. 13 and 14—note the values of  $G_L \cdot R \times a^2$  at  $z/a = x/a = 0$ . This fact can also be deduced from the steady-state temperature distributions in Fig. 8. The temperature gradients at the solid-liquid interface increase with decreasing values of uniform absorbed heat flux  $q$ .

For given values of  $qa$  and  $Ua/2\alpha$  the cooling rate continuously decreases toward the edges of the metal pool, Figs. 13 and 14. This is expected since both the temperature gradient in the  $y$ -direction and the solid-liquid interface velocity perpendicular to itself tend to



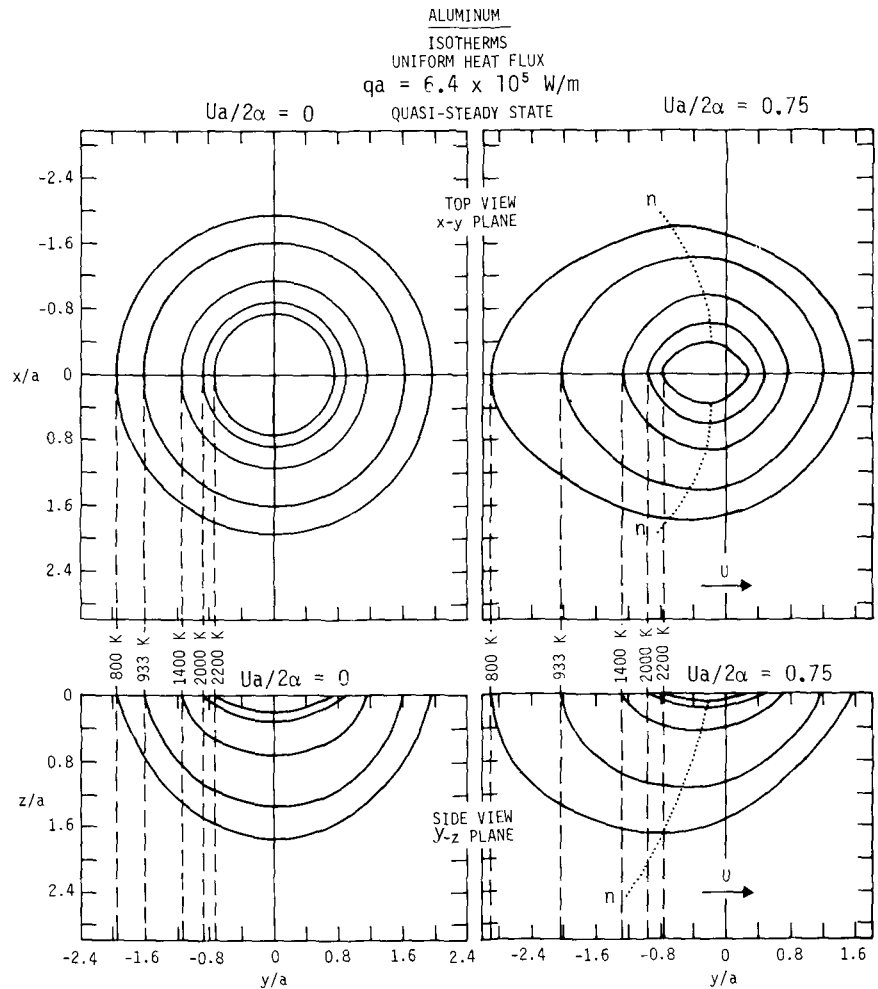


Fig. 10—Composite side and top views of the isotherms in an aluminum substrate subjected to stationary and moving uniform absorbed heat fluxes over a circular region on its boundary surface. The  $n-n$  curve connects the points of maximum temperature farthest from the  $y$ -axis.

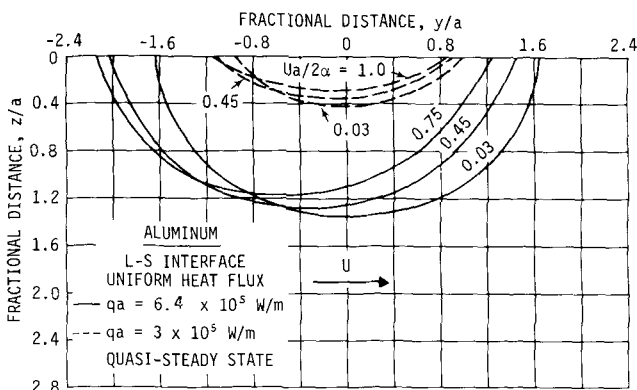


Fig. 11—A side view,  $x = 0$  plane, showing the effects of changing the values of  $qa$  and  $Ua/2\alpha$  on the shape and size of the molten region.

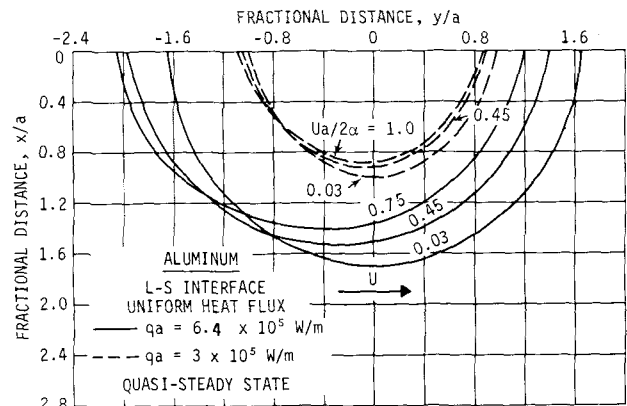


Fig. 12—A top view,  $z = 0$  plane, showing the effects of changing the values of  $qa$  and  $Ua/2\alpha$  on the shape and size of the molten region.

zero at points of maximum melt depth and melt width, in other words no melting occurs at these locations. Examples of cooling rates that are readily calculated from these figures are as follows. Assume a uniform heat flux of  $q = 1.2 \times 10^9 \text{ W/m}^2$  absorbed over circular region of radius  $a = 250 \mu\text{m}$  is moving with a velocity  $U \sim 0.5 \text{ m/s}$ ,  $qa \sim 3 \times 10^5 \text{ W/m}$  and  $Ua/2\alpha \sim 0.75$ . The calculated cooling rates from Figs. 13 and 14 at  $y/a = 0$ ,  $x/a = 0.8$  and  $z/a = 0.4$  are  $\sim 9 \times 10^6 \text{ K/s}$ ,  $\sim 3.7 \times 10^6 \text{ K/s}$  and  $\sim 8 \times 10^4 \text{ K/s}$ , respectively.

The ratio of the temperature gradient in the liquid at

and perpendicular to the solid-liquid interface divided by the solid-liquid interface velocity perpendicular to the melt pool during solidification,  $G_L/R$ , is a measure of the stability of a planar interface and its progressive breakdown into cellular and dendritic solidification modes. This parameter is plotted vs the  $z/a$  and  $x/a$  axis for different values of the variables  $qa$  and  $Ua/2\alpha$  in Figs. 15 and 16, respectively. The data clearly indicate that the minimum  $G_L/R$  value consistently occurs along the centerline of the moving pool on the  $y/a$  axis. The interface velocity at this location is in the

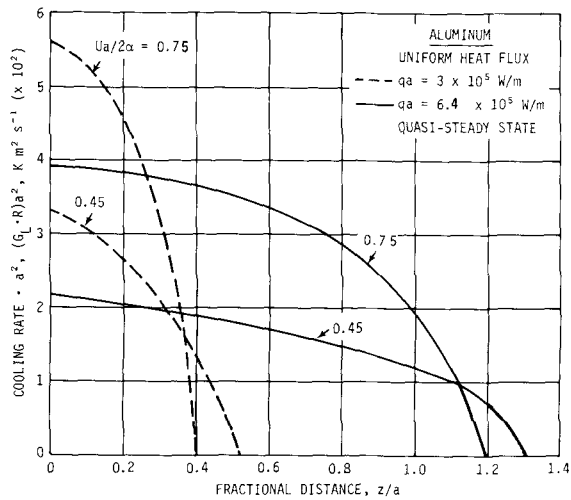


Fig. 13—Variation of the product of cooling rate at the solid-liquid interface and  $a^2$  with melt depth along the trailing half of the pool in the  $x = 0$  plane for different values of the independent process variables.

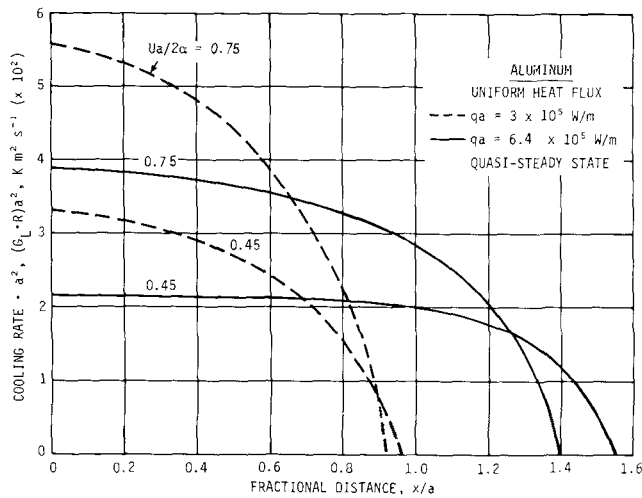


Fig. 14—Variation of the product of cooling rate at the solid-liquid interface and  $a^2$  with melt width along the side of the pool in the  $z = 0$  plane for different values of the independent process variables.

$y$ -direction and assumes its maximum value of  $U$ . At a given dimensionless velocity  $Ua/2\alpha$  the temperature gradient  $G_L$  and the ratio  $G_L/R$  in this location decrease with increasing value of the product  $qa$ . Similarly, at a given value of  $qa$  increasing the traverse speed of the heat source results in a corresponding decrease in  $G_L/R$ .

It is important to note that as one moves along the back of the pool on the  $x = 0$  plane from  $z/a = 0$  toward the bottom of the pool the interface velocity vector both rotates and changes in magnitude—it starts out at its maximum value of  $U$  pointing in the positive  $y$ -direction and continuously decreases to zero at the maximum pool depth. It is thus clear why the  $G_L/R$  increases with increasing distance down the back of the pool, increasing  $z/a$ , Fig. 15.

In a similar manner, simultaneous rotation and decrease in magnitude of the interface velocity vector

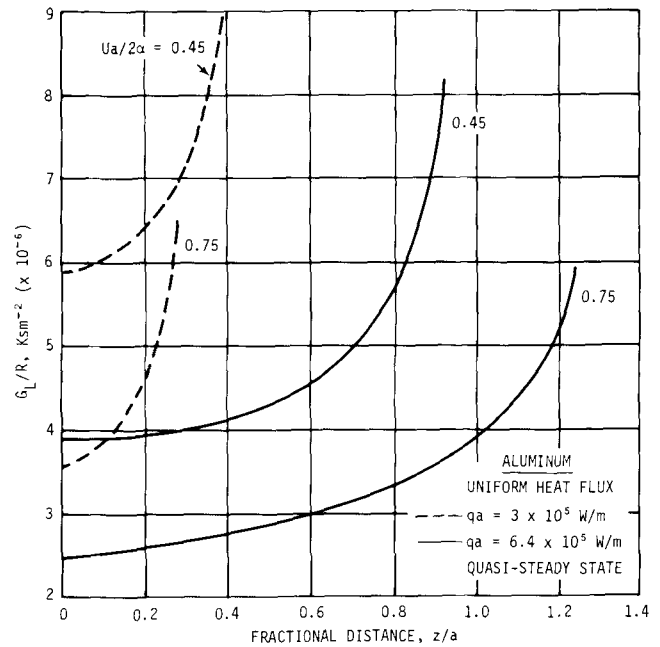


Fig. 15—Variation of the ratio  $G_L/R$  at the solid-liquid interface with melt depth along the trailing half of the pool in the  $x = 0$  plane for different values of the independent process variables.

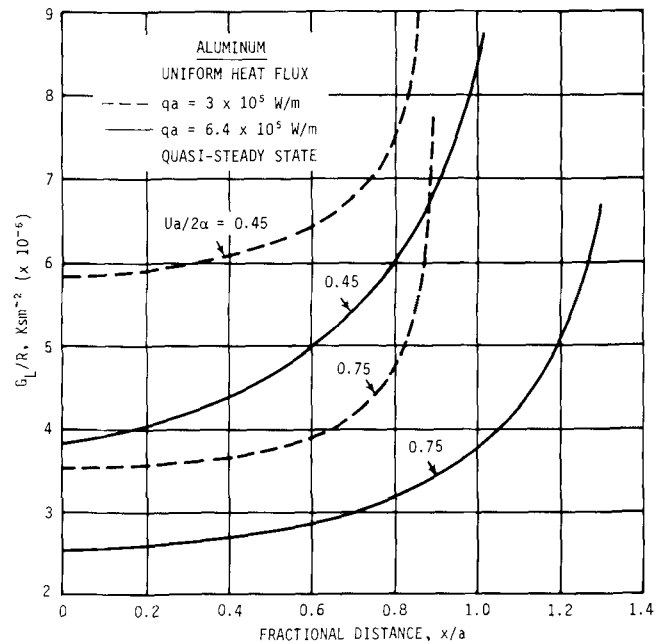


Fig. 16—Variation of the ratio  $G_L/R$  at the solid-liquid interface with the melt width along the side of the pool in the  $z = 0$  plane for different values of the independent process variables.

occurs in the  $z = 0$  plane as one moves from the back to the side of the pool. This explains the increasing  $G_L/R$  values with increasing distance along  $x/a$  in Fig. 16.

**B. Gaussian Heat Flux.** The effect of changing the heat flux distribution from a top hat (uniform) to a Gaussian was investigated. As previously noted,<sup>2</sup> if the total absorbed power in the circular region,  $Q$ , is identical for the uniform and the Gaussian heat flux distributions, then the following relationship is readily

deduced:

$$q_{\text{uniform}} = \frac{q_0}{2.313} \quad [38]$$

where  $q_0$  is the absorbed heat flux at the center of the circular region in the Gaussian distribution.

Examples of calculated liquid-solid interface locations for the Gaussian heat flux distributions are shown in Figs. 17 and 18. The product  $q_0 a / 2.313 \sim 4.65 \times 10^5$  W/m resulted in a maximum steady state  $T(0,0,0) = T_v$  for the case of a stationary heat source. This value is lower than that for the uniform heat flux due to the high concentration of absorbed power at the center of the Gaussian distribution. The liquid-solid interface for small values of the dimensionless velocity  $Ua/2\alpha$  is symmetrical in both the  $y = 0$  and  $z = 0$  planes, Figs. 17 and 18, respectively. For a given temperature in the center of the circular region the metal pool is shallower for the Gaussian heat flux distribution—compare the solid curve for  $Ua/2\alpha \sim 0.03$  in Fig. 17 with the curve

for  $qa = 6.4 \times 10^5$  for the same dimensionless velocity in Fig. 11. This is expected since the total power absorbed in the Gaussian distribution is lower.

Decreasing the product  $q_0 a / 2.313$  results in colder and shallower melt pools while increasing the dimensionless velocity shifts the trailing end of the pool toward the negative  $y$ -axis. These observations are in line with previous findings for the case of uniform heat flux. It was also found that motion of the heat source has a more pronounced influence on the melt temperatures than in the previous case. For example, increasing the dimensionless interface velocity to  $Ua/2\alpha \sim 0.75$  reduced the temperature at  $T(0,0,0)$  from  $T_v$  to  $\sim 1600$  K for the value of  $q_0 a / 2.313 \sim 4.65 \times 10^5$  W/m.

Finally, general trends relating cooling rates and  $G_L/R$  values are similar to those previously discussed for the case of uniform absorbed heat flux distribution.

## VI. SUMMARY

The three-dimensional temperature distributions in the melt pool and the adjacent heat affected zone of a semi-infinite substrate subjected to a moving directed high energy source can be readily determined with the generalized formulation of the heat flow equation in orthogonal curvilinear coordinates coupled to an enthalpy model. While numerical computations are presented for an aluminum substrate subjected to moving uniform and Gaussian heat flux distributions, the equations developed could be equally applicable to a range of metallurgical processes previously treated with the moving point source equation. It is shown that if the two independent variables  $qa$  and  $Ua/2\alpha$  or  $U/q$  are specified, the dimensionless temperature distributions in a given substrate material remain the same. Shortcomings of the model include the use of constant thermophysical properties and the fact that convection in the metal pool is not taken into consideration except by arbitrarily increasing its thermal conductivity. On the other hand, the general trends that can be deduced for a given energy source and substrate material should permit a more systematic approach to the variation and control of the process variables in order to achieve the desired heat flow conditions during melting and solidification.

## APPENDIX

An alternate method to the general formulation of the finite difference representation of the heat conduction equation in moving orthogonal curvilinear coordinate system, Eq. [1], is considered here. In this method an energy balance is applied to a control volume of finite size in oblate spheroidal coordinates moving with velocities  $v_\eta$ ,  $v_\xi$  and  $v_\phi$ , see Fig. 2. The resultant energy balance is approximated using finite differences and is shown to converge to an identical formulation as that given in Eqs. [9] and [10]. This approach is used to both verify the general formulation of Eq. [1] developed in this investigation and to render improved physical interpretation of the various coefficients given in Eq. [10].

The moving control volume element about a point

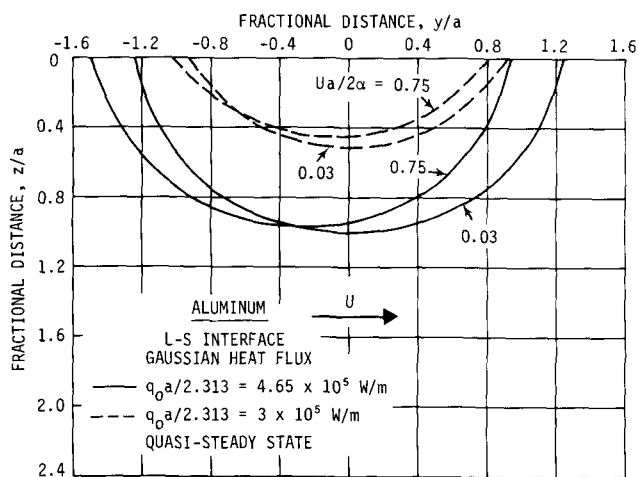


Fig. 17—A side view,  $x = 0$  plane, showing the effects of changing the values of  $qa$  and  $Ua/2\alpha$  on the shape and size of molten region of an aluminum substrate subjected to a Gaussian heat flux moving with constant velocity  $U$  in the positive  $y$ -direction.

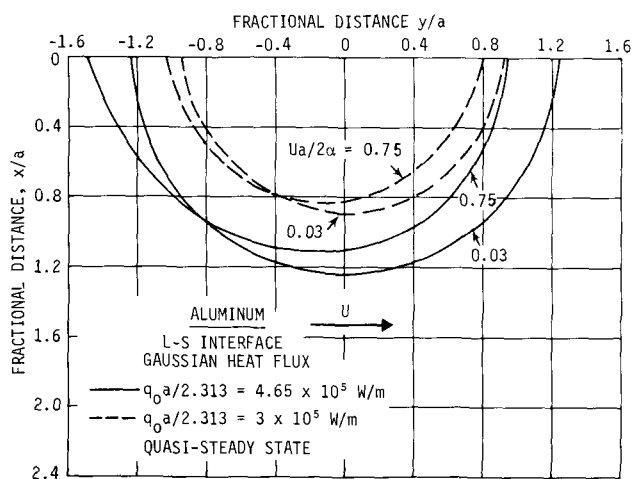


Fig. 18—A top view,  $z = 0$  plane, showing the effects of changing the values of  $qa$  and  $Ua/2\alpha$  on the shape and size of the molten region of an aluminum substrate subjected to a Gaussian heat flux moving with constant velocity  $U$  in the positive  $y$ -direction.

$(i, j, k)$  is illustrated in Fig. 2. The energy balance for this volume element having a total source strength of  $P\Delta V$  is carried out by considering the total rate of heat transfer through each surface by conduction and due to the motion of the volume element.

Let  $Q$  and  $Q'$  denote the rate of heat transfer entering or leaving the volume element by conduction and by motion of the volume element, respectively. The energy balance for the quasisteady state case under consideration is given by:

$$\begin{aligned} & (Q_{i-1/2,j,k} - Q_{i+1/2,j,k}) \\ & + (Q_{i,j-1/2,k} - Q_{i,j+1/2,k}) \\ & + (Q_{i,j,k-1/2} - Q_{i,j,k+1/2}) \\ & + (Q'_{i+1/2,j,k} - Q'_{i-1/2,j,k}) \\ & + (Q'_{i,j+1/2,k} - Q'_{i,j-1/2,k}) \\ & + (Q'_{i,j,k+1/2} - Q'_{i,j,k-1/2}) \\ & + P\Delta V = 0 \end{aligned} \quad [A1]$$

In what follows the values of  $Q$  and  $Q'$  for the  $i - 1/2$  and  $i + 1/2$  faces are evaluated as examples. All the other terms in Eq. [A1] can then be similarly obtained. It is shown that the sum of all these terms, after appropriate manipulations, results in Eq. [9] with the coefficients defined in Expression [10].

$$Q_{i-1/2,j,k} = -k \frac{(T_{i,j,k} - T_{i-1,j,k})}{(\Delta S_{\eta})_{i-1/2}} \Delta A_{i-1/2} \quad [A2]$$

Appropriate substitutions of Eqs. [2] to [4] and the appropriate form of the scalar factors for oblate spheroidal coordinate system into Eq. [A2] and some manipulation gives:

$$\begin{aligned} Q_{i-1/2,j,k} &= -C_1 (T_{i,j,k} - T_{i-1,j,k}) \\ &\quad \times ak \cosh \eta_i \sin \xi_j \Delta \eta \Delta \xi \Delta \phi \end{aligned} \quad [A3]$$

Similarly,

$$\begin{aligned} Q_{i+1/2,j,k} &= -C_2 (T_{i+1,j,k} - T_{i,j,k}) \\ &\quad \times ak \cosh \eta_i \sin \xi_j \Delta \eta \Delta \xi \Delta \phi \end{aligned} \quad [A4]$$

The coefficients  $C_1$  and  $C_2$  are those defined in Expression [10]. Similar expressions to [A3] and [A4] are readily developed for the rates of heat transfer through the other four faces of the volume element due to conduction.

The rate of heat transfer entering the  $i - 1/2$  face due to the motion of the volume element is:

$$Q'_{i-1/2,j,k} = \rho C_p T_{i-1/2,j,k} v_{\eta_{i-1/2}} \Delta A_{i-1/2} \quad [A5]$$

Substitution of Eqs. [3], the appropriate form of the scalar factors and [8] into Eq. [A5] gives:

$$\begin{aligned} Q'_{i-1/2,j,k} &= \frac{aU\rho C_p \sin \xi_j \sin \phi_k}{k\Delta \eta} [T_{i-1/2,j,k}] \\ &\quad \cdot \frac{\sinh \eta_{i-1/2} \cosh \eta_{i-1/2}}{\cosh \eta_i} \\ &\quad \cdot ak \cosh \eta_i \sin \xi_j \Delta \eta \Delta \xi \Delta \phi \end{aligned} \quad [A6]$$

$$\begin{aligned} Q'_{i-1/2,j,k} &= \frac{aU\rho C_p \sin \xi_j \sin \phi_k}{k\Delta \eta} (T_{i-1/2,j,k}) \\ &\quad \cdot ak \cosh \eta_i \sin \xi_j \Delta \eta \Delta \xi \Delta \phi \\ &\quad \cdot \left[ \sinh \eta_i - \frac{\cosh 2\eta_i}{\cosh \eta_i} \frac{\Delta \eta}{2} \right] \end{aligned} \quad [A7]$$

Similarly:

$$\begin{aligned} Q'_{i+1/2,j,k} &= \frac{aU\rho C_p \sin \xi_j \sin \phi_k}{k\Delta \eta} (T_{i+1/2,j,k}) \\ &\quad \cdot ak \cosh \eta_i \sin \xi_j \Delta \eta \Delta \xi \Delta \phi \\ &\quad \cdot \left[ \sinh \eta_i + \frac{\cosh 2\eta_i}{\cosh \eta_i} \frac{\Delta \eta}{2} \right] \end{aligned} \quad [A8]$$

Subtraction of Eq. [A7] from [A8] gives:

$$\begin{aligned} & Q'_{i+1/2,j,k} - Q'_{i-1/2,j,k} \\ &= \frac{aU\rho C_p \sin \xi_j \sin \phi_k \cdot ak \cosh \eta_i \sin \xi_j \Delta \eta \Delta \xi \Delta \phi}{k} \\ &\quad \cdot \left[ \frac{\sinh \eta_i}{2\Delta \eta} (T_{i+1/2,j,k} - T_{i-1/2,j,k}) + \frac{\cosh 2\eta_i}{\cosh \eta_i} (T_{i,j,k}) \right] \end{aligned} \quad [A9]$$

Substituting Eqs. [A3], [A4], [A9] and similar terms for the other four faces into Eq. [A1] and dividing both sides by

$$ak \cosh \eta_i \sin \xi_j \Delta \eta \Delta \xi \Delta \phi$$

gives an identical equation to Expression [9]. Note that the sum of the second terms inside the brackets of Eq. [A9], the coefficient to  $T_{i,j,k}$ , becomes zero in Eq. [A1]. This essentially implies that the sum of the combination of area and velocity terms multiplied and differentiated with respect to each axis is zero or

$$\sum_{n=1}^3 \frac{\partial}{\partial u_n} \left( \frac{\rho C_p h v_n}{h_n} \right) = 0 \quad [A10]$$

which is the continuity requirement.

## NOMENCLATURE

$a$	radius of the circular region, m or $\mu\text{m}$
$A$	area of the element
$C$	integration constant
$C_p$	specific heat, $\text{JKg}^{-1}\text{K}^{-1}$
$f_l$	fraction liquid
$G_L$	temperature gradient in the liquid at the liquid-solid interface, $\text{Km}^{-1}$
$h$	scalar factor
$H$	specific enthalpy, $\text{JKg}^{-1}$
$\Delta H_{st}$	heat of fusion, $\text{JKg}^{-1}$
$k$	thermal conductivity, $\text{Jm}^{-1}\text{s}^{-1}\text{K}^{-1}$
$P$	rate of heat generation per unit volume, $\text{Wm}^{-3}$
$q$	absorbed heat flux, $\text{Wm}^{-2}$
$Q$	rate of total absorbed heat, W
$R$	interface velocity, $\text{ms}^{-1}$
$s$	arc length
$t$	time, s
$T$	temperature, K

$T_o$  ambient temperature, K  
 $T_M$  melting temperature, K  
 $T_v$  vaporization temperature, K  
 $u$  coordinate axis  
 $U$  velocity of heat source,  $\text{ms}^{-1}$   
 $V$  volume,  $\text{m}^3$   
 $v$  velocity,  $\text{ms}^{-1}$   
 $x, y, z$  cartesian coordinates  
 $\alpha$  thermal diffusivity ( $k/\rho C_p$ ),  $\text{m}^2\text{s}^{-1}$   
 $\eta, \xi, \phi$  oblate spheroidal coordinates  
 $\theta$  dimensionless temperature variable  
 $\psi$  dimensionless enthalpy variable  
 $\rho$  density,  $\text{Kg M}^{-3}$

#### Subscripts

$i, j, k$  nodal point subscripts in  $\eta$  and  $\xi$  and  $\phi$  directions, respectively.

#### ACKNOWLEDGMENT

This research was sponsored by the Defense Advanced Research Projects Agency under the overall direction of Dr. E. C. van Reuth and was monitored

by the Office of Naval Research under Contract Number N00014-78-C-0275. Technical monitor of the contract was Dr. B. A. MacDonald.

#### REFERENCES

1. S. C. Hsu, S. Chakravorty, and R. Mehrabian: *Met. Trans. B*, 1978, vol. 9B, p. 221.
2. S. C. Hsu, S. Kou, and R. Mehrabian: *Met. Trans. B*, 1980, vol. 11B, p. 29.
3. D. Rosenthal: *Weld. J.*, 1941, vol. 20, Research Supplement, p. 2205.
4. G. E. Schneider, A. B. Strong, and M. M. Yovanovich: *Proceedings of International Symposium on Computer Methods for Partial Differential Equations*, R. Vichnevetsky, ed., pp. 312-17, AICA, New Brunswick, NJ, 1975.
5. F. B. Hilderbrand: *Advanced Calculus for Applications*, Prentice-Hall, Inc., Englewood Cliffs, NJ, 1962.
6. N. Shamsunder and E. M. Sparrow: *J. Heat Transfer*, 1975, p. 333.
7. G. Horvay and J. W. Cahn: *Acta Metall.*, 1961, vol. 9, p. 695.
8. G. E. Nash and M. E. Glicksman: *Acta Metall.*, 1974, vol. 22, p. 1283.